The Climatic Role of Interactive Leaf Phenology in the Vegetation-Atmosphere System of Radiative-Convective Equilibrium Storm-Resolving Simulations

Tellus B
Chemical and Physical Meteorology

ORIGINAL RESEARCH PAPER

JUNHONG LEE
CATHY HOHENEGGER
ANDREAS CHLOND
REINER SCHNUR

*Author affiliations can be found in the back matter of this article

STOCKHOLM UNIVERSITY PRESS

ABSTRACT

Storm-resolving simulations where deep convection can be explicitly resolved are performed in the idealized radiative-convective equilibrium framework to explore the climatic role of interactive leaf phenology. By initializing the system with different initial soil moisture and leaf area index (LAI) conditions, we find three categories of potential equilibrium climatic and vegetation states: a hot desert planet without vegetation, an intermediate sparsely vegetated planet, and a wet fully vegetated planet. The wet fully vegetated equilibrium category occurs over the widest range of initial soil moisture as it occurs as soon as soil saturation is 19% higher than the permanent wilting point (35%). This indicates that a quite harsh environment is needed in our modeling system to force leaves to be shed. The attained equilibrium states are only dependent upon the initial soil moisture, not the initial LAI. However, interactive leaves do allow an earlier transition from the intermediate to the wet vegetated equilibrium category. Hence, interactive leaves make the vegetation-atmosphere system more stable and more resilient to drying. This effect could be well approximated by just prescribing the LAI to its maximum value. Finally, our sensitivity experiments reveal that leaves influence the climate equally through their controls on canopy conductance and vegetation cover, whereas albedo changes play a negligible role.

CORRESPONDING AUTHOR:

Junhong Lee

Max Planck Institute for Meteorology, Hamburg, Germany

junhong.lee@mpimet.mpg.de

KEYWORDS:

equilibrium states; leaf phenology; storm-resolving simulations; radiative-convective equilibrium; hydrological cycle

TO CITE THIS ARTICLE:

Lee, J, Hohenegger, C, Chlond, A and Schnur, R. 2022. The Climatic Role of Interactive Leaf Phenology in the Vegetation-Atmosphere System of Radiative-Convective Equilibrium Storm-Resolving Simulations. *Tellus B: Chemical and Physical Meteorology*, 74(2022), 164–175. DOI: https://doi.org/10.16993/tellusb.26

1. INTRODUCTION

Leaf phenology refers to the temporal evolution of leaf amount due to leaf emergence, growth, and death. Leaf amount is usually described by leaf area index (LAI) in climate or numerical weather prediction models. The LAI governs canopy conductance, vegetation cover, and albedo. Through this, the LAI influences evapotranspiration, sensible heat flux, surface temperature and boundary layer structure, and ultimately climate. For example, the greening of the earth's surface due to global warming can increase evapotranspiration and induce cooling at the surface (Zeng et al., 2017; Piao et al., 2020). Feedbacks between temperature and leaf phenology, when leaves are allowed to respond to changing atmospheric conditions interactively, amplify heatwaves in summer in a regional climate model (Stéfanon et al., 2012). In addition to its impact on heatwaves, it is also known that leaf phenology plays a critical role in drought (Wolf et al., 2016). Therefore, interactive leaves are an essential component to understand vegetation-atmosphere interactions.

These past studies have employed coarse-resolution simulations with grid spacing larger than O(10 km) to quantify the effects of interactive leaves on climate. Yet interactions between leaf phenology and atmospheric processes involve small-scale processes that are either not included or parameterized in such models. On the vegetation side, Wang and Eltahir (2000) reported that errors in LAI and vegetation cover due to ignored subgrid variability in precipitation can propagate into the atmosphere again, leading to significantly different vegetation and atmospheric states. On the atmospheric side, Hohenegger et al. (2009) showed that by explicitly resolving convection instead of parameterizing it, possible with a grid spacing of a few kilometers, feedbacks between soil moisture and precipitation changed sign, from positive (with parameterized convection) to negative. This suggests a weaker impact of land alterations on the atmosphere that coarser-resolution climate models might have implied. Models with kilometer-scale grid spacing, which are now well established for weather forecasting and regional climate simulations, nevertheless have not been used to investigate the importance of interactive leaves for climate.

In this study, we investigate the effects of interactive leaves on the determination of the equilibrium climate of an idealized planet and the resulting equilibrium vegetation states using kilometer-scale simulations that can explicitly resolve deep convection. We tackle this problem from three angles. First, we characterize potential equilibrium climatic states, including the state of their vegetation, by varying both the initial LAI and the initial soil moisture. We here not only vary the initial LAI for given initial soil moisture, but also the initial soil moisture to quantify the range of soil moistures that support leaves at equilibrium. Second, we deduce the climatic effects of interactive leaves by comparing simulations with interactive leaves to those with fixed LAI. Third, we assess the relative importance of the LAI control on canopy conductance, vegetation cover and albedo for the derived equilibrium states. In order to achieve these goals, we take advantage of the radiative-convective equilibrium (RCE) framework that, given the homogeneity of the set-up, allows us to conduct long enough simulations on a small domain with high enough horizontal grid spacing to resolve deep convection. Past RCE studies (especially, Becker and Stevens, 2014; Rochetin et al., 2014; Cronin et al., 2015; Hohenegger and Stevens, 2018) have shown the usefulness of this conceptualization to understand aspects of the climate system involving land-atmosphere interactions. As a model, we employ the ICOsahedral Nonhydrostatic (ICON) model (Zängl et al., 2015) with Jena Scheme for Biosphere-Atmosphere Coupling in Hamburg (JSBACH, Reick et al., 2021) as the land component. The model is run at a grid spacing of 2.5 km.

Although past studies have not directly looked at the potential existence of equilibria in the climate system just due to the presence of interactive leaves, several studies have looked at the question of equilibria by varying the initial soil moisture or by allowing species to die, live and colonize new geographical areas depending on the climatic conditions. This is not possible in our set-up. A plant cannot colonize new areas where it was previously not present. It can only increase or decrease the area of its leaves. From these past studies, Brovkin et al. (1998) found that a desert or a green equilibrium state is possible over the Sahara when using a general circulation model coupled with a biome model, both run at a resolution of 5.6°. With a simple box model, D'Andrea et al. (2006) explained the existence of dry and wet equilibrium states by purely varying the initial soil moisture. By coupling an ecological model to the box model of D'Andrea et al. (2006), Baudena et al. (2008) reported the existence of a hot and desert state as well as of a wet and vegetated state. Recently, Aleina et al. (2013) found an additional in-between equilibrium state, dry and cool by adding a second atmospheric and a second soil layer in their box model. It will thus be interesting to see whether by only allowing leaves to interact with the climate, such equilibrium states are possible and whether the resulting effects on the climate are of similar magnitude.

This study is structured as follows: Section 2 describes the model and the configuration of the experiments. Section 3 characterizes the equilibrium states and investigates the potential existence of equilibria in the vegetation-atmosphere system. Section 4 discusses the importance of interactive leaves. Lastly, section 5 summarizes the results.

2 MODEL DESCRIPTION

2.1 MODEL

We use the ICON model in an idealized set-up. The physical parameterizations that we employ include the 3D Smagorinsky turbulence scheme for horizontal and vertical turbulent mixing (Smagorinsky, 1963), a single-moment microphysics scheme to predict rain water, cloud water, cloud ice, snow, and graupel (Seifert, 2008), an all-or-nothing cloud fraction scheme to represent the effect of clouds on radiative processes (Sommeria and Deardorff, 1977), the RRTMG radiation (PSrad) package for longwave and shortwave radiative transfer calculations (Pincus and Stevens, 2013), and the land component JSBACH to represent land surface processes. Since our simulations employ a grid spacing of 2.5 km, as detailed below, we do not use a convection scheme, neither for shallow nor for deep convection. The ICON model has been employed in the past to simulate the atmospheric flow at kilometer-scale and finer resolutions, see e.g., Becker et al., 2018; Stevens et al., 2019; Hohenegger et al., 2020. As it is nevertheless the first time that this specific set of parameterizations is employed for high-resolution simulations, especially combining JSBACH to the Smagorinsky turbulence scheme, we document the ability of our configuration to reproduce well-known idealized case studies of boundary layer development in the appendix.

Given the focus of this study on the role of interactive leaves, we introduce here briefly how the latter are handled in JSBACH for the case of the C3 grass, which is the only plant functional type that we are considering (see section 2.2). The growth and shed of vegetation and, hence the LAI, are determined by soil moisture, temperature, and net primary productivity as

$$\frac{dLAI}{dt} = \begin{cases} kLAI\left(1-\dfrac{LAI}{LAI_{max}}\right) & \text{for} T_s > 4\ ^{\circ}\text{C}, \theta > \theta_{pwp}, \\ & \text{and } NPP > 0 \\ -pLAI & \text{otherwise,} \end{cases} \quad (1)$$

where LAI_{max} = 3.0 m^2 m^{-2} is the physiological maximum limit, k = 9.0 · 10^{-2} d^{-1} is the growth rate, p = 1.5 · 10^{-2} d^{-1} is the shed rate, T_s is the surface temperature, θ is soil moisture, θ_{pwp} is the permanent wilting point, and *NPP* is the net primary productivity which is computed considering photosynthesis and the respiration of the vegetation. The LAI then influences three vegetation properties. Those are canopy conductance (g_c), vegetation cover (C_v), and albedo (α). Canopy conductance is obtained as

$$g_c = \begin{cases} A_c \cdot f_{ws} \cdot \dfrac{1.6}{c_a - c_i}\dfrac{RT}{p} & \text{for} q_a < q_s \\ 0 & \text{otherwise,} \end{cases} \quad (2)$$

where A_c is total assimilation in canopy, f_{ws} is a scaling factor depending on the relative soil moisture in the root zone, c_a is the CO_2 concentration in the air, c_i is the leaf internal CO_2 concentration given by c_i = 0.87 c_a according to Knorr (1997), R is the universal gas constant, T is air temperature, p is surface pressure, q_a is specific humidity of air, and q_s is saturation specific humidity at the surface. f_{ws} is computed as

$$f_{ws} = \begin{cases} 0 & \text{for} \theta \le \theta_{pwp} \\ \dfrac{\theta - \theta_{pwp}}{\theta_{crit} - \theta_{pwp}} & \text{for} \theta_{pwp} < \theta < \theta_{crit} \\ 1 & \text{otherwise,} \end{cases} \quad (3)$$

where θ_{crit} = 0.2775 m^3 m^{-3}. Here, A_c is a function of LAI according to

$$A_c = \int_0^{LAI} A(l)dl, \quad (4)$$

where A is the total carbon fixation in unit of LAI. A itself is a function of photosynthesis and of the respiration of the vegetation. Vegetation cover is given by

$$C_v = C_{v,max}\left(1 - e^{-LAI/k_c}\right), \quad (5)$$

where $C_{v,max}$ is the maximum cover of vegetation, set to 1 in our study, and k_c = 2 is a characterization constant representing the random orientation of leaves. Finally, the albedo is computed as

$$\alpha_{vis} = (1 - C_v) \cdot \alpha_{soil,vis} + C_v \cdot \alpha_{can,vis}, \quad (6)$$

$$\alpha_{nir} = (1 - C_v) \cdot \alpha_{soil,nir} + C_v \cdot \alpha_{can,nir}, \quad (7)$$

$$\alpha = \frac{\alpha_{vis} \cdot SW_{\downarrow,vis} + \alpha_{nir} \cdot SW_{\downarrow,nir}}{SW_{\downarrow,vis} + SW_{\downarrow,nir}}, \quad (8)$$

where α is albedo, $SW_{\downarrow}$ is downward shortwave radiation, subscripts *vis* and *nir* are for visible and near-infrared ranges, subscripts *soil* and *can* refer to soil and canopy. In our configuration, $\alpha_{soil,vis}$ = 0.15, $\alpha_{soil,nir}$ = 0.26, $\alpha_{can,vis}$ = 0.08, and $\alpha_{can,nir}$ = 0.33, respectively. Consequently, changes in leaf phenology can induce changes in transpiration (T_r), bare soil evaporation (E_b) and, hence, evapotranspiration (ET) directly via changes in canopy conductance and vegetation cover, and indirectly via changes in albedo according to

$$T_r = C_v \cdot \rho \frac{q_a - q_s}{r_a + 1/g_c}, \quad (9)$$

$$E_b = (1 - C_v) \cdot \rho \frac{q_a - hq_s}{r_a}, \quad (10)$$

$$ET = T_r + E_b, \quad (11)$$

where r_a is aerodynamic resistance and h is the relative humidity of the top soil. The detailed description of JSBACH can be found in Reick et al. (2021).

2.2 EXPERIMENTAL SET-UP

Our model configuration uses a pseudo 2-D torus grid with doubly periodic lateral boundary on a domain of 40 by 40 grid points. We use such a small domain to avoid that convection begins to self-organize, which is known to strongly affect the mean atmospheric properties (Bretherton et al., 2005; Muller and Held, 2012). We use a storm-resolving resolution of 2.5 km, with 63 vertical layers and a model top at 27 km. The model is integrated for 360 days with a configuration of RCE, see especially Hohenegger and Stevens (2018) who already performed 3D storm-resolving RCE simulations with an interactive land surface for a comprehensive description of the set-up. In short, the model starts from homogeneous boundary and surface conditions. There is no rotation and the insolation is spatially uniform. The insolation varies diurnally with an averaged value of 340 W m^{-2}.

We choose the values of the parameters for the land surface processes according to Hohenegger and Stevens (2018) and modify some of them as required by the use of a more complex land surface scheme. We assume that C3 grass is the only plant functional type covering the surface motivated by the fact that 1) it is ubiquitous over the globe, especially dominant in arid and semi-arid regions (Patriarca et al., 2019), 2) it reacts to soil moisture perturbations rapidly, and 3) its phenological phase has no seasonal dependency. Root depth is set to 1 m in our simulation, a typical value for grass. We use loam as soil type, which is a typical soil type in the presence of grass, unlike Hohenegger and Stevens (2018) who used loamy clay for their bare soil simulations. Accordingly, we use a heat capacity of $2.25 \cdot 10^2$ J m^{-3} K^{-1} and a thermal diffusivity of $7.4 \cdot 10^{-1}$ m^2 s^{-1} corresponding to loam soil type. We assume a soil of 1 m depth consisting of two soil layers with 0.1 m for the top soil and 0.9 m for the deep soil and initial soil moisture is stored only in the deep soil layer as in Aleina et al. (2013). This allows both for a fast thermal response of the top soil layer and permits the grass to tap into a deeper water reservoir making this soil moisture available to the atmosphere. If plant transpiration is reduced (e.g., due to small LAI), then only bare soil evaporation from the top soil layer can transfer water from the soil into the atmosphere and this may not be sufficient to maintain the hydrological cycle. The condition of our setup is similar to that of the dry season in continental mid-latitudes or to drought conditions in Europe as well as to semi-arid and arid conditions (Baudena et al., 2008). Field capacity (θ_{fc}) and permanent wilting point are set to 0.37 and 0.1295 m^3 m^{-3}, in the range of expected values for loamy soils. Finally, we neglect the surface runoff and gravitational drainage at the bottom of the deep soil to ensure water conservation in the system as in Hohenegger and Stevens (2018).

In order to investigate the climatic role of interactive leaves, we perform 12 experiments by initializing the system with different soil moisture and LAI. We combine six different initial soil moisture (θ_0) values of 0.1, 0.15, 0.2, 0.25, 0.3, and 0.35 m^3 m^{-3} with two different initial values of LAI of 0.4 and 3.0 m^2 m^{-2}. These two values represent the seed value and maximum possible value of LAI for grass. Table 1 lists these experiments where we name them after their initial LAI and soil moisture with the prefix 'INT' to indicate the experiments are with interactive leaves. Note that we will use soil saturation ($\theta/\theta_{fc} \cdot 100\%$) rather than volumetric water content in the remainder of the text. To further understand the importance of interactive leaves for the equilibrium climate, we perform 12 supplementary experiments keeping the LAI fixed at its initial value. We also name the supplementary experiments after their initial LAI and soil moisture but with the prefix 'FIX' instead of 'INT'. Finally, to clarify which of canopy conductance, vegetation cover and albedo mostly controls the effect of LAI on evapotranspiration and climate, we perform three additional sensitivity experiments (Table 2). For the first experiment, we fix the LAI in the equations for canopy conductance (Eq. 2) to 0.4 m^2 m^{-2}. For the second and third experiments, we fix the LAI in the equation for vegetation cover (Eq. 5) and albedo (Eqs. 6–8) to 0.4 m^2 m^{-2}. Remember that 0.4 m^2 m^{-2} is the seed value of LAI

EXPERIMENT NAME	LAI_0 (m^2 m^{-2})	θ_0 (m^3 m^{-3})	θ_0 (%)
INT_LAI04_SM27	0.4	0.10	27
INT_LAI04_SM41	0.4	0.15	41
INT_LAI04_SM54	0.4	0.20	54
INT_LAI04_SM68	0.4	0.25	68
INT_LAI04_SM81	0.4	0.30	81
INT_LAI04_SM95	0.4	0.35	95
INT_LAI30_SM27	3.0	0.10	27
INT_LAI30_SM41	3.0	0.15	41
INT_LAI30_SM54	3.0	0.20	54
INT_LAI30_SM68	3.0	0.25	68
INT_LAI30_SM81	3.0	0.30	81
INT_LAI30_SM95	3.0	0.35	95

Table 1 List of conducted experiments with interactive leaves defined by their initial values of LAI, of soil moisture, and of soil saturation.

EXPERIMENT NAME	VARIABLE THAT HAS FIXED LAI AT 0.4 m^2 m^{-2}
INT_LAI04_SM54_gc	g_c, canopy conductance
INT_LAI04_SM54_cv	C_v, vegetation fraction
INT_LAI04_SM54_a	α, albedo

Table 2 List of conducted sensitivity experiments.

for grass and thus corresponds to the lowest possible LAI value when conditions are favorable for growth. Using this value in Eqs. 5, 6 and 7 results in a vegetation cover fixed at 0.18 for the second experiment and an albedo for visible and near-infrared ranges fixed at 0.14 and 0.27 for the third experiment.

3 EQUILIBRIA IN THE VEGETATION-ATMOSPHERE SYSTEM WITH INTERACTIVE LEAVES

In this section, we focus on simulations with interactive leaves and characterize the possible equilibrium states of our idealized planet by varying both initial LAI and initial soil saturation. We assume that each simulation reaches an equilibrium state once its precipitation is equal to evapotranspiration. These equilibrium states from each simulation are classified into three equilibrium categories based on their LAI being minimum, maximum, or in-between. Thus, each individual equilibrium state in a given category shares the same broad climate and vegetation characteristics, although the attained individual values can be slightly different.

From past studies that have made use of other types of modeling framework (see introduction), we expect three climatic equilibrium categories as a function of initial soil saturation for a given initial LAI. Thus, these simulations with different initial soil moisture will allow us to quantify the resulting equilibrium LAI values and the range of soil saturation that supports leaves. A priori, we would expect the existence of at least one climatic equilibrium category with leaves fully shed and one with full leaves coverage. Of particular interest is thus whether one of these three expected climatic equilibrium categories is associated with an in-between value of LAI.

Figure 1 shows the evolution to equilibrium for three representative simulations. In our vegetation-atmosphere system, the water budget in most of the simulations quickly equilibrates, with precipitation being equal to evaporation already after 30 days and at most after 50 days. Concerning the surface temperature, slight warming or cooling trends are still visible after 360 days in some of the simulations. We nevertheless assume that equilibrium has been achieved as the variations in surface temperature are small after 300 days and the hydrological cycle is the main driver of the vegetation-atmosphere system. Thus for our subsequent analysis, we focus on the last 60 days of the simulation period.

Figure 2 shows LAI, evapotranspiration and surface temperature at equilibrium for the various simulations. Note that at equilibrium, evapotranspiration equals precipitation. Three climatic equilibrium categories exist: 1) a hot desert equilibrium category without leaves when $\theta_0 \leq 27\%$, 2) a sparsely vegetated equilibrium category when $27\% < \theta_0 < 54\%$, and 3) a wet fully vegetated

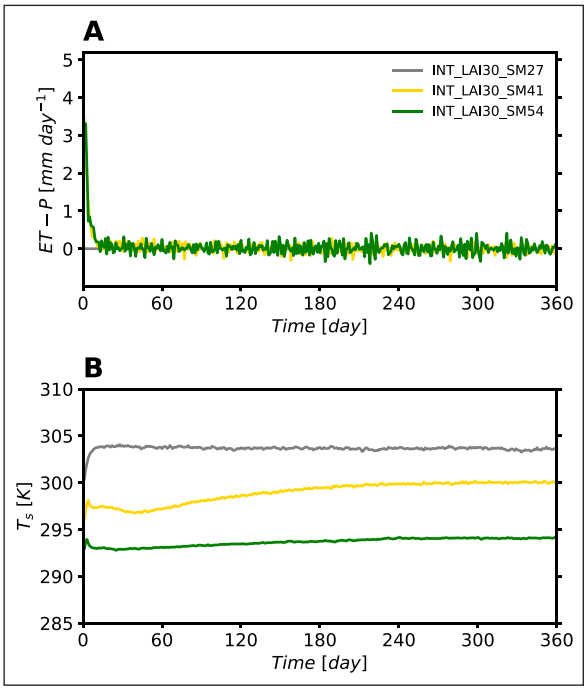

Figure 1 Time series of **(a)** the difference between evapotranspiration (*ET*, mm day^{-1}) and precipitation (*P*, mm day^{-1}), and **(b)** surface temperature (T_s, K) for INT_LAI30_SM27 (gray), INT_LAI30_SM41 (yellow), and INT_LAI30_SM54 (green).

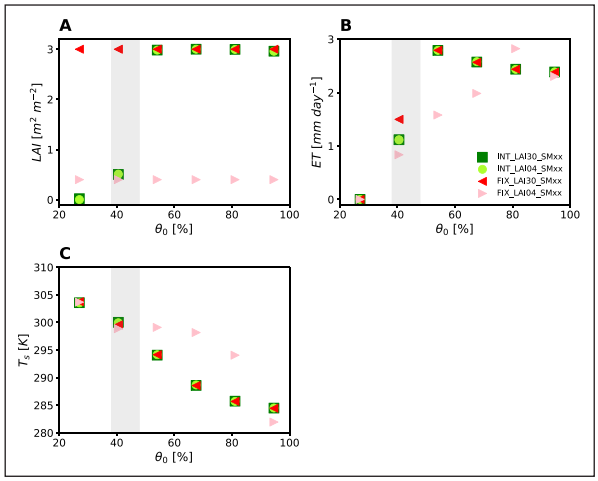

Figure 2 (a) Leaf area index (LAI, m^2 m^{-2}), **(b)** evapotranspiration (*ET*, mm day^{-1}), and **(c)** surface temperature (T_s, K) as a function of initial soil saturation (θ_0, %) at equilibrium for INT_LAI04_SMxx (light green circles), INT_LAI30_SMxx (dark green squares), FIX_LAI04_SMxx (light red triangles), and FIX_LAI30_SMxx (dark red triangles). The gray area indicates the sparsely vegetated equilibrium category.

equilibrium category when $\theta_0 \geq 54\%$. The attained equilibrium states are dependent upon the chosen initial soil saturation, not the initial LAI (compare dark green squares and light green circles, see further below).

In the hot desert equilibrium category, all leaves of the vegetation are shed, surface temperature is 303.6 K and precipitation is close to zero at equilibrium (Figure 2). The initial soil saturation is too low to support vegetation ($\theta_0 < \theta_{pwp}$) and spins up the hydrological cycle. Thus, even when starting from a high LAI, vegetation starts to shed its

leaves as soon as the simulation starts and transpiration does not occur at equilibrium (Figure 3). Also, bare soil evaporation is limited by the low soil moisture content. This logically results in a hot and dry state at equilibrium that belongs to the hottest and driest of the three equilibrium categories.

The sparsely vegetated equilibrium category is the in-between category where every characteristic of the system takes intermediate values (Figure 2). Initial soil saturation is high enough to support evapotranspiration and precipitation (1.12 mm day^{-1}) leading to a cooler surface (300.0 K), but not large enough to maintain a fully vegetated surface. To determine the precise soil saturation range of the sparsely vegetated category, we perform supplementary experiments. The initial soil moisture of these supplementary experiments ranges from 0.11 to 0.19 m^3 m^{-3} (from 30% to 51%) in increment of 0.01 m^3 m^{-3} with an initial LAI of 3 m^2 m^{-2}. According to the results of our supplementary experiments, the sparsely vegetated category is an unlikely category in the sense that LAI reaches the in-between value at equilibrium only for a small range of soil saturation, in our model for initial soil saturations between precisely 38 to 49% (the gray area in Figure 2). Variations in soil saturation between 38 to 49% result in slight variations in the equilibrium values of LAI, evapotranspiration and surface temperature, but their ranges of values are still in-between values. Evapotranspiration increases from 0.48 to 2.60 mm day^{-1} and LAI increases from 0.36 to 2.81 m^2 m^{-2} when initial soil saturation increases from 38 to 49%. Surface temperature decreases from 300.0 to 295.8 K.

The wet fully vegetated equilibrium category is the equilibrium category having fully grown vegetation, precipitation up to 3 mm day^{-1} and a cooler land surface (T_s < 294.1 K) (Figure 2). The initial soil saturation is high enough to let vegetation grow, the vegetation can tap into the deep soil water reservoir, and there is enough water in this reservoir and to maintain it. The contribution of transpiration to evapotranspiration is 0.90 mm day^{-1} larger than the one of bare soil evaporation, since most of the surface is covered by vegetation ($C_v \approx 0.77$) (Figure 3). Here note that, even though the surface is fully vegetated, vegetation cover is only ~ 0.77 and not 1. This results from the value given by Eq. 5 when LAI equals its maximum value.

For the wet fully vegetated equilibrium category, evapotranspiration starts to slightly decrease from 2.79 to 2.39 mm day^{-1} when initial soil saturation increases from 54 to 95%. This is because evapotranspiration in this equilibrium category is in the energy-limited regime, where net radiation, rather than soil moisture, is the major controlling factor (Seneviratne et al., 2010). In our simulation, net radiation is reduced when initial soil saturation is high, explaining the decrease in evapotranspiration (Figure 4). The reduction in net radiation can be explained by an increased cloud amount, blocking downward shortwave radiation. Even though downward longwave radiation can be theoretically larger in a moister and cloudier atmosphere and thus compensates for reduced downward shortwave radiation, downward longwave radiation is also decreased due to the colder temperatures in the planetary boundary layer as soil saturation increases. The decrease in precipitation is also consistent with weaker radiative cooling. When initial soil saturation increases from 54 to 95%, radiative cooling decreases from 108.5 to 105.1 W m^{-2}.

Comparison of the different simulations with interactive leaves in Figure 2 also indicates how easy it is to make plants shed their leaves in our modeling framework. It is actually quite difficult to make plants shed their leaves. The LAI stays at its minimum value only if the initial soil saturation is less than 38%, which is very close to the permanent wilting point (35%). In contrast, the wet equilibrium category occurs over the widest range of initial soil saturation among the states as it occurs for initial soil saturation larger than 54%. Expressed in terms of soil moisture index $(\theta_0 - \theta_{pwp})/(\theta_{fc} - \theta_{pwp})$, leaves do not grow only for a soil moisture index smaller than 0.044, whereas equilibrium state falls into the wet equilibrium category for a soil moisture index larger than 0.293. From this, we conclude that the vegetation can survive under a relatively dry atmosphere. If our results would be transferable to the question of Amazon dieback, they would imply that the Amazon forest is more resilient to perturbations and that we are further away from a potential tipping point than generally thought. Studies with coarse-resolution earth system models and dynamic vegetation seem to indicate dieback of the Amazon forest already by a small drying,

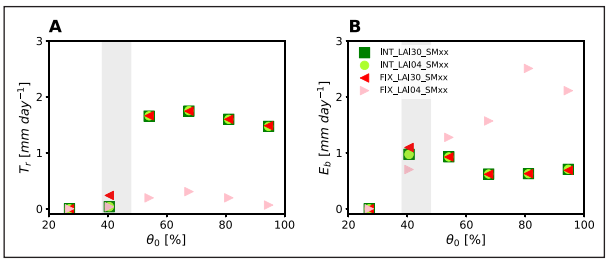

Figure 3 Same as Figure 2 but for **(a)** transpiration (T_r, mm day^{-1}) and **(b)** bare soil evaporation (E_b, mm day^{-1}).

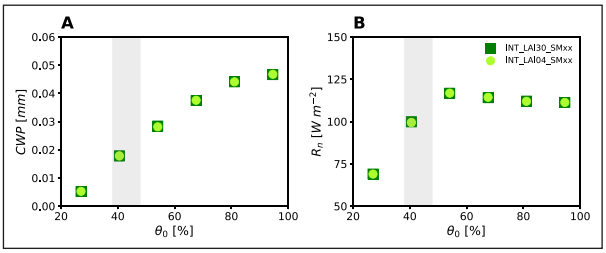

Figure 4 Same as Figure 2 but for **(a)** cloud water path (*CWP*, mm) and **(b)** surface net radiation (R_n, W m^{-2}) only for the simulations with interactive leaves.

much smaller than what was found here for C3 grass. For instance, tipping point of tropical forest was found to range from 2.7 to 3 mm day^{-1} (Cox et al., 2004; Hirota et al., 2011; Staal et al., 2018). In our study, even if we do not carry out simulations with tropical forest, leaves are fully shed below a soil saturation of 38%, where the mean precipitation drops to 1.12 mm day^{-1}. This is well below the 2.7 mm day^{-1} threshold from these other studies. The differences could come from the different plant functional types or indicate an oversensitivity of vegetation to drying in coarse-resolution climate models. To clarify this, it would be interesting to redo our experiments using tropical forest as plant functional type, a topic let for further study.

Finally, Figure 2 indicates that the attained equilibrium states are only dependent on the initial soil saturation and not on the initial LAI, as can be seen by comparing pairs of simulations with initial LAI values of 0.4 and 3 m^2 m^{-2} for given initial soil saturation values. This indicates that the initial value of soil saturation dictates the equilibrium state belonging to the dry or wet equilibrium category and the LAI follows. A small initial value of LAI cannot induce a dry state under wet initial soil saturation conditions as the leaves end up growing. The initial value of LAI alone cannot cause an equilibrium state to move into a different equilibrium category. This is different from what has been found in Aleina et al. (2013), where a small initial value of vegetation cover always leads to a dry state, independently of the initial soil saturation. Remember that in our simulations the vegetation cover can only change through variations in LAI and not by plants colonizing or retreating from geographical areas, as in Aleina et al. (2013).

Despite this difference, our three equilibrium categories are qualitatively similar to that of Aleina et al. (2013). In Aleina et al. (2013), the air temperature averaged over the lower 1 km decreases by 8 K during the transition from the desert state to the fully vegetated state. Our study shows a cooling by 15.9 K. Precipitation increases by 0.64 mm day^{-1} in Aleina et al. (2013), whereas it is increased by as much as 2.55 mm day^{-1} in our simulation. These numbers suggest a stronger sensitivity of the vegetation-atmosphere system in our modeling framework. This may relate to the fact that we explicitly simulate atmospheric processes, whereas Aleina et al. (2013) used convective parameterization and only two atmospheric layers. Another difference between the two studies is that our intermediate equilibrium category still has vegetation whereas Aleina et al. (2013) do not have any. This is because the vegetation in Aleina et al. (2013) do not use top soil moisture in their simple model.

Given the conceptual nature of our study, it is difficult to compare our findings to observations of land-atmosphere interactions. The RCE conceptualization is generally thought to best represent mean climatic conditions over the tropical areas (Manabe and Strickler, 1964) and the mean precipitation amount obtained in the fully vegetated equilibrium category of 3 mm day^{-1} in our study coincides with the mean precipitation amount as observed over tropical land area. We also note that the in-between sparsely vegetated equilibrium category only occurs in our model for soil saturation of 38 to 49%. Such values are generally found in the Sahel, which may also be seen as sparsely vegetated (Patriarca et al., 2019).

4 THE ROLE OF INTERACTIVE LEAVES

We explore the importance of interactive leaves by performing two sets of sensitivity experiments. First, we compare the equilibrium states of simulations with and without interactive leaves for given initial soil saturation and LAI conditions. Second, we investigate which of the controls of LAI on canopy conductance, vegetation cover, and albedo mainly affects the equilibrium state of the vegetation-atmosphere system.

Comparing the simulation with and without interactive leaves in Figure 2 indicates that interactive leaves allow an earlier transition from the sparsely vegetated equilibrium category to the fully vegetated equilibrium category. With interactive leaves, this transition happens at a soil saturation of 54%, whereas it happens at a soil saturation of 81% for the cases when the LAI is prescribed to its minimum. Through this, precipitation can be up to 77% larger with interactive leaves (by θ_0 = 54%) and the surface more than 9.6 K (by θ_0 = 68%) colder. These differences can be mainly explained by the fact that the vegetation with larger LAI tends to have larger canopy conductance and vegetation cover, and smaller albedo resulting in larger evapotranspiration and precipitation. Similarly, Baudena et al. (2008) reported that the probability of being in the fully vegetated equilibrium state tends to be increased with the effect of plant colonization. The delayed transition from the fully vegetated equilibrium category to the sparsely vegetated equilibrium category with decreasing initial soil saturation implies that interactive leaves make the vegetation-atmosphere system more stable and more resilient to drying.

Although taking into account interactive leaves is important in the case of wet soils, this is only true with respect to the simulation using the prescribed minimum LAI value. Comparison of the simulations with interactive leaves to the ones using the prescribed maximum LAI shows no difference, as the vegetation rapidly grows in the simulation with interactive leaves to reach its maximum value. In fact, the simulations using the prescribed maximum LAI are always close to the ones using interactive leaves. From this, we conclude that using a value of LAI prescribed at its maximum may be a good first-order approximation and a better approximation than fixing the LAI to another value.

Figure 5 quantifies the contribution of canopy conductance, vegetation cover, and albedo to the changes induced in the equilibrium state by interactive leaves. We focus on the simulation with initial soil saturation of 54%, which displayed the largest sensitivity as compared to the simulation using a fixed LAI of 0.4 m^2 m^{-2}. Letting canopy conductance and vegetation cover vary with interactive leaves but fixing the albedo to its value in FIX_LAI04_SM54 leads to similar values of evapotranspiration and surface temperature as in INT_LAI04_SM54, where canopy conductance, vegetation cover, and albedo are allowed to vary. Hence we conclude that albedo changes due to interactive leaves play no role. Rather, it is found that the enhancement of evapotranspiration with interactive leaves results from the increase in canopy conductance as well as in vegetation cover. The albedo decreases from 0.2019 in INT_LAI04_SM54 to 0.2008 in INT_LAI04_SM54_a at equilibrium when LAI reaches 3 m^2 m^{-2}, indicating a small sensitivity of albedo to LAI in our vegetation-atmosphere system. In contrast, the value of canopy conductance at equilibrium is 3.87 mm s^{-1} in INT_LAI04_SM54, which is 3.37 mm s^{-1} larger than that of INT_LAI04_SM54_gc, and results in a 0.76 mm day^{-1} increase in evapotranspiration. Vegetation cover increases from 0.18 to 0.77 with interactive leaves, increasing evapotranspiration by about 0.54 mm day^{-1}. A larger vegetation cover means a larger contribution from transpiration than from bare soil evaporation to evapotranspiration. Since transpiration is generally larger than bare soil evaporation, this translates itself into an increase in evapotranspiration. The sum of evapotranspiration decreases when individually fixing albedo, canopy conductance and vegetation cover is 1.3 mm day^{-1} and this value is similar to the difference between INT_LAI04_SM54 and FIX_LAI04_SM54, 1.21 mm day^{-1}. This indicates that interactive leaves influence the equilibrium climate mostly through canopy conductance and vegetation cover and nonlinear interactions play a minor role.

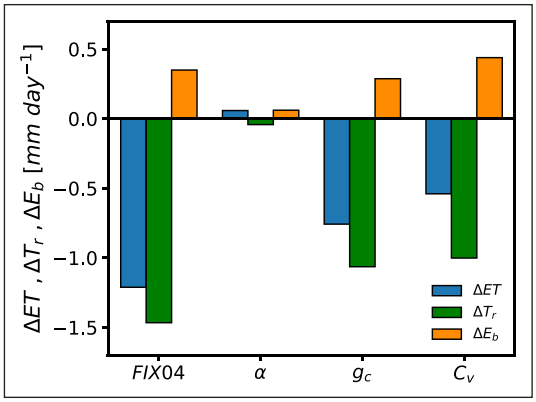

Figure 5 Differences in evapotranspiration, transpiration and bare soil evaporation between INT_LAI04_SM54 and FIX_LAI04_SM54, denoted as FIX04 on the x-axis, as well as the differences between INT_LAI04_SM54 and the three sensitivity experiments INT_LAI04_SM54_gc, INT_LAI04_SM54_cv, INT_LAI04_SM54_a, denoted g_c, C_v and α on the x-axis.

Previous studies that have only considered an interactively varying vegetation cover, Baudena et al. (2008) and Aleina et al. (2013), also reported that changes in albedo play an insignificant role even when increasing the difference between soil albedo and canopy albedo. The sensitivity of evapotranspiration to canopy conductance has been investigated in van Heerwaarden and Teuling (2014) for an idealized case of moist boundary layer growth. In their sensitivity tests, changing the LAI of grassland from 3 to 5 m^2 m^{-2} induced an increase in evapotranspiration smaller than 1.04 mm day^{-1}. This is similar to our result where an increase in LAI from 0.4 to 3 m^2 m^{-2} induces a 0.76 mm day^{-1} increase in evapotranspiration. The importance of the control of LAI on vegetation cover has also been noted by Vivoni (2012). Using remotely sensed and hydrology model data over shrubland and savannas, they showed that the ratio of transpiration to evapotranspiration increases from 0.01 to 0.31 as a result of a vegetation cover increase from 0.05 to 0.58. In our study, the ratio is increased from 0.29 to 0.60, while the vegetation cover increases from 0.18 to 0.77.

5 SUMMARY AND CONCLUSION

Changes in leaf phenology feed back on land-atmosphere interactions and the climate system through the leaf control on evapotranspiration. Here, in contrast to past studies, we explore such effects using simulations that can explicitly resolve deep convection. We are particularly interested to understand what are possible equilibrium vegetation (or rather leaves) states in dependence on initial soil moisture and to which degree the presence of interactive leaves affects the equilibrium characteristics.

To that aim, we employ the conceptualization of radiative-convective equilibrium (RCE), where interactions between leaves and the climate can be studied in a simplified way and over a small domain, the latter allowing us to conduct long enough integrations until equilibrium has set in. To perform RCE simulation, the ICON model is used. As the land component of ICON, JSBACH represents interactive leaves as changes of LAI, which impacts canopy conductance, vegetation cover and albedo, and hence evapotranspiration. We choose the parameters for the land surface processes according to Hohenegger and Stevens (2018) and modify some of them due to the presence of vegetation and interactive leaves. Especially, we focus on C3 grass for plant functional type due to its fast response time and its widespread occurrence on Earth.

With this configuration, we conduct simulations with and without interactive leaves by spanning different

initial soil saturation and initial LAI conditions. Our results and findings may be summarized as follows:

- Three climatic and vegetation equilibrium categories are possible in dependence of initial soil saturation: a hot desert equilibrium category with LAI at its minimum, an intermediate sparsely vegetated equilibrium category and a wet fully vegetated equilibrium category with LAI at its maximum. The wet fully vegetated equilibrium category occurs over the widest range of initial soil moisture. It occurs for initial soil saturation values higher than 54%, whereas the hot desert equilibrium category requires soil saturation below 38%, close to the permanent wilting point (35%). As such, making plants shed their leaves is quite difficult in our modelling framework.
- The attained equilibrium states are only dependent on the initial soil saturation and not on the initial LAI. Variation in initial LAI alone cannot push an equilibrium state to move into a different equilibrium category.
- Interactive leaves lead to an earlier transition to the wet fully vegetated equilibrium category, by a soil saturation of 54% against 81% when LAI is fixed at its minimum value. This suggests that interactive leaves stabilize the system and make it more resilient to drying. Differences are nevertheless inexistent when comparing to simulations with LAI fixed at its maximum value as interactive leaves rapidly grow to their maximal area. This indicates that in terms of modeling, prescribing LAI to its maximum value seems sufficient to capture the effect of interactive leaves and a better approximation than prescribing it to its minimum value.
- Leaves affect the climate almost equally through their effect on canopy conductance and vegetation cover, whereas albedo changes play a negligible role.

APPENDIX A

The validation of the 3D Smagorinsky turbulence scheme newly implemented in ICON is described here. Two physics packages are available in the ICON model: one for numerical weather prediction (NWP version), which includes the Smagorinsky turbulence scheme but no leaf phenology model, and one for climate modeling, which includes leaf phenology but a turbulence scheme designed for coarser-resolution applications based on total turbulence energy (TTE scheme, Mauritsen et al., 2007; Pithan, 2014). We thus implemented the 3D Smagorinsky scheme in the climatic version of ICON. The Smagorinsky scheme is especially suitable for simulations at large-eddy resolution, with a grid spacing of O(100 m), but has also been used in previous studies (Bretherton et al. 2005; Tompkins and Semie, 2017) of RCE conducted with a grid spacing of O(1 km).

We evaluate the implemented scheme by comparing it to the ICON NWP version (Dipankar et al., 2015) and to the original ICON configuration using the TTE scheme. For this evaluation, we use an idealized configuration of a convective boundary layer growing in a stable layer, following past studies, especially Dipankar et al. (2015) who implemented the 3D Smagorinsky scheme in the NWP version of the ICON model. The configuration uses a 2D torus grid with doubly periodic lateral boundary conditions, on a domain of 96 by 96 grid points. The horizontal resolution is 100 m and the model top is 3.2 km with 64 vertical layers. The surface heat flux is fixed at 0.1 K m s^{-1} (120.6 W m^{-2}) and the latent heat flux at 0.00008 m s^{-1} (240.1 W m^{-2}), providing the boundary layer with energy to grow. Slight differences to the set-up used by Dipankar et al. (2015) exist, namely that 1) the integration is done for 6 hours, 2) we have surface latent heat flux, and 3) the humidity profile is taken from the idealized simulations of Stevens (2007). To ensure that the three considered versions of ICON are identical in their set-up except for the turbulence scheme, we switched off other parameterizations (i.e., microphysics and radiation). The results will be shown by averaging spatially over the domain and temporally over the last 15 minutes of the simulation with 30 seconds sampled data.

Figure A1 shows profiles of domain-averaged potential temperature and specific humidity at six hours. Our scheme shows profiles similar to the NWP configuration whereas the version with the TTE scheme displays much stronger mixing and a too deep planetary boundary layer. This can be explained by the fact that turbulence schemes

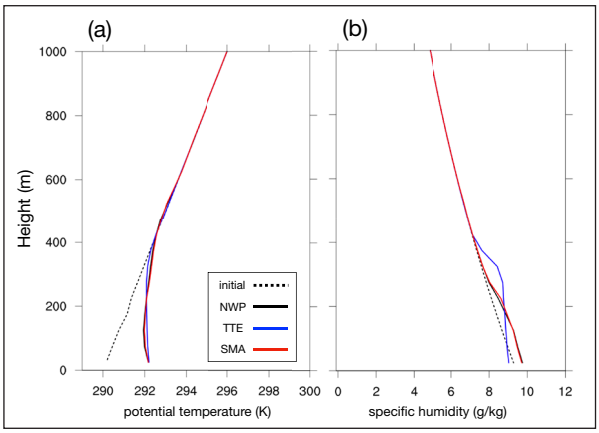

Figure A1 Domain mean profiles of **(a)** potential temperature and **(b)** specific humidity at the initial time (dashed line) and at 6 hours for total turbulent energy scheme denoted TTE (blue line), 3D Smagorinsky scheme in the NWP version denoted NWP (black), and the newly implemented 3D Smagorinsky scheme denoted SMA (red).

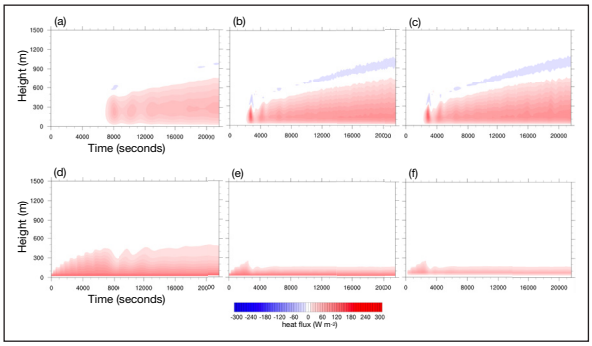

Figure A2 Time series of (**a**, **b**, and **c**) resolved and (**d**, **e**, and **f**) sub-grid scale heat flux (shading, W m^{-2}) using (**a**, **d**) total turbulent energy scheme, (**b**, **e**) 3D Smagorinsky scheme in the NWP physics package, and (**c**, **f**) the newly implemented 3D Smagorinsky scheme.

designed for coarser-resolution simulations tend to have a fixed ratio of subgrid-scale mixing to total mixing (Shin and Dughia, 2016), and hence produce excessive subgrid-scale mixing even if the required amount of mixing is already resolved at a grid spacing of O(100 m). Indeed, as shown by Figure A2, the subgrid-scale heat flux for the TTE scheme is too strong and reaches a much higher altitude as compared to the Smagorinsky scheme. Furthermore, it was later found that the TTE scheme employed an erroneous and too large mixing length, also in agreement with and contributing to the displayed too strong mixing. In contrast, the newly implemented Smagorinsky scheme simulates both the resolved scale heat flux and the entrainment process well. It also shows weaker subgrid-scale heat flux, as expected, all in better agreement with the NWP results. Slight differences with the NWP results remain. They might stem from the use of distinct implicitness factor in the temporal discretization to solve the vertical diffusion equation (e.g., Eq 2.192 in Giorgetta et al., 2013). Our scheme uses 1.5 for the implicitness factor whereas the NWP version uses 1.0.

ACKNOWLEDGEMENTS

The study was supported by the Max Planck society for the advancement of science. We thank Hao-Wei Wey for the internal review and the comments by one reviewer that help strengthen and clarify our manuscript. The simulations were performed using the facilities of the DKRZ (Deutsches Klimarechenzentrum). Primary data and scripts used in the analysis and other supporting information that may be useful in reproducing the author's work can be obtained from http://hdl.handle.net/21.11116/0000-0009-4A52-8.

COMPETING INTERESTS

The authors have no competing interests to declare.

AUTHOR AFFILIATIONS

Junhong Lee orcid.org/0000-0001-6459-9284
Max Planck Institute for Meteorology, Hamburg, Germany
Cathy Hohenegger orcid.org/0000-0002-7478-6275
Max Planck Institute for Meteorology, Hamburg, Germany
Andreas Chlond
Max Planck Institute for Meteorology, Hamburg, Germany
Reiner Schnur
Max Planck Institute for Meteorology, Hamburg, Germany

REFERENCES

Aleina, CF, Baudena, M, D'Andrea, F and **Provenzale, A.** 2013. Multiple equilibria on planet dune: climate–vegetation dynamics on a sandy planet. *Tellus B.* 65(1): 17662. DOI: https://doi.org/10.3402/tellusb.v65i0.17662

Baudena, M, D'Andrea, F and **Provenzale, A.** 2008. A model for soil- vegetation-atmosphere interactions in water-limited ecosystems. *Water Resour. Res.* 44(12): W12429. DOI: https://doi.org/10.1029/2008WR007172

Becker, T, Bretherton, CS, Hohenegger, C and **Stevens, B.** 2018. Estimating bulk entrainment with unaggregated and aggregated convection. *Geophys. Res. Lett.* 45(1): 455–462. DOI: https://doi.org/10.1002/2017GL076640

Becker, T and **Stevens, B.** 2014. Climate and climate sensitivity to changing CO_2 on an idealized land planet. *J. Adv. Model. Earth Syst.* 6(4): 1205–1223. DOI: https://doi.org/10.1002/2014MS000369

Bretherton, CS, Blossey, PN and **Khairoutdinov, M.** 2005. An energy-balance analysis of deep convective self-aggregation above uniform sst. *J. Atmos. Sci.* 62(12): 4273–4292. DOI: https://doi.org/10.1175/JAS3614.1

Brovkin, V, Claussen, M, Petoukhov, V and **Ganopolski, A.** 1998. On the stability of the atmosphere-vegetation system in the sahara/sahel region. *J. Geophys. Res.* 103(D24): 31613–31624. DOI: https://doi.org/10.1029/1998JD200006

Cox, PM, Betts, R, Collins, M, Harris, PP, Huntingford, C and **Jones, C.** 2004. Amazonian forest dieback under climate-carbon cycle projections for the 21st century. *Theoretical and applied climatology.* 78(1): 137–156. DOI: https://doi.org/10.1007/s00704-004-0049-4

Cronin, TW, Emanuel, KA and **Molnar, P.** 2015. Island precipitation enhancement and the diurnal cycle in radiative-convective equilibrium. *Q. J. R. Meteorol. Soc.* 141(689): 1017–1034. DOI: https://doi.org/10.1002/qj.2443

D'Andrea, F, Provenzale, A, Vautard, R and **De Noblet-Decoudré, N.** 2006. Hot and cool summers: Multiple equilibria of the continental water cycle. *Geophys. Res. Lett.* 33(24). DOI: ttps://doi.org/10.1029/2006GL027972

Dipankar, A, Stevens, B, Heinze, R, Moseley, C, Zängl, G, Giorgetta, M and **Brdar, S.** 2015. Large eddy simulation using the general circulation model icon. *J.*

Adv. Model. Earth Syst. 7(3): 963–986. DOI: https://doi.org/10.1002/2015MS000431

Giorgetta, MA, Roeckner, E, Mauritsen, T, Bader, J, Crueger, T, Esch, M, Rast, S, Kornblueh, L, Schmidt, H, Kinne, S, et al. 2013. The atmospheric general circulation model echam6-model description.

Hirota, M, Holmgren, M, Van Nes, EH and **Scheffer, M.** 2011. Global resilience of tropical forest and savanna to critical transitions. *Science.* 334(6053): 232–235. DOI: https://doi.org/10.1126/science.1210657

Hohenegger, C, Brockhaus, P, Bretherton, CS and **Schär, C.** 2009. The soil moisture–precipitation feedback in simulations with explicit and parameterized convection. *J. Clim.* 22(19): 5003–5020. DOI: https://doi.org/10.1175/2009JCLI2604.1

Hohenegger, C, Kornblueh, L, Klocke, D, Becker, T, Cioni, G, Engels, JF, Schulzweida, U and **Stevens, B.** 2020. Climate statistics in global simulations of the atmosphere, from 80 to 2.5 km grid spacing. *J. Meteorol. Soc.* Japan. DOI: https://doi.org/10.2151/jmsj.2020-005

Hohenegger, C and **Stevens, B.** 2018. The role of the permanent wilting point in controlling the spatial distribution of precipitation. *Proc. Natl. Acad. Sci.* 115(22): 5692–5697. DOI: https://doi.org/10.1073/pnas.1718842115

Knorr, W. 1997. *Satellitengestützte Fernerkundung und Modellierung des Globalen CO2-Austauschs der Landvegetation: Eine Synthese*. PhD thesis. University of Hamburg Hamburg.

Manabe, S and **Strickler, RF.** 1964. Thermal equilibrium of the atmosphere with a convective adjustment. *J. Atmos. Sci.* 21(4): 361–385. DOI: https://doi.org/10.1175/1520-0469(1964)021<0361:TEOTAW>2.0.CO;2

Mauritsen, T, Svensson, G, Zilitinkevich, SS, Esau, I, Enger, L and **Grisogono, B.** 2007. A total turbulent energy closure model for neutrally and stably stratified atmospheric boundary layers. *J. Atmos. Sci.* 64(11): 4113–4126. DOI: https://doi.org/10.1175/2007JAS2294.1

Muller, CJ and **Held, IM.** 2012. Detailed investigation of the selfaggregation of convection in cloud-resolving simulations. *J. Atmos. Sci.* 69(8): 2551–2565. DOI: https://doi.org/10.1175/JAS-D-11-0257.1

Patriarca, C, Bako, M, Branthomme, A, Frescino, TS, Haddad, FF, Hamid, AH, Martucci, A, Chour, HO, Patterson, PL, Picard, N, et al. 2019. Trees, forests and land use in drylands: The first global assessment. *FAO Forestry Paper No. 184*. Rome, Italy: Food and Agriculture Organization of the United Nations, 184 p.

Piao, S, Wang, X, Park, T, Chen, C, Lian, X, He, Y, Bjerke, JW, Chen, A, Ciais, P, Tømmervik, H, et al. 2020. Characteristics, drivers and feedbacks of global greening. *Nat. Rev. Earth Environ.* 1(1): 14–27. DOI: https://doi.org/10.1038/s43017-019-0001-x

Pincus, R and **Stevens, B.** 2013. Paths to accuracy for radiation parameterizations in atmospheric models. *J. Adv. Model. Earth Syst.* 5(2): 225–233. DOI: https://doi.org/10.1002/jame.20027

Pithan, F. 2014. *Arctic boundary-layer processes and climate change*. PhD thesis. Universität Hamburg Hamburg.

Reick, CH, Gayler, V, Goll, D, Hagemann, S, Heidkamp, M, Nabel, JE, Raddatz, T, Roeckner, E, Schnur, R and **Wilkenskjeld, S.** 2021. Jsbach 3-the land component of the mpi earth system model: documentation of version 3.2.

Rochetin, N, Lintner, BR, Findell, KL, Sobel, AH and **Gentine, P.** 2014. Radiative–convective equilibrium over a land surface. *J. Clim.* 27(23): 8611–8629. DOI: https://doi.org/10.1175/JCLI-D-13-00654.1

Seifert, A. 2008. A revised cloud microphysical parameterization for cosmo-lme. *COSMO Newsletter.* 7: 25–28.

Seneviratne, SI, Corti, T, Davin, EL, Hirschi, M, Jaeger, EB, Lehner, I, Orlowsky, B and **Teuling, AJ.** 2010. Investigating soil moisture–climate interactions in a changing climate: A review. *Earth- Sci. Rev.* 99(3–4): 125–161. DOI: https://doi.org/10.1016/j.earscirev.2010.02.004

Shin, HH and **Dudhia, J.** 2016. Evaluation of pbl parameterizations in wrf at subkilometer grid spacings: Turbulence statistics in the dry convective boundary layer. *Mon. Wea. Rev.* 144(3): 1161–1177. DOI: https://doi.org/10.1175/MWR-D-15-0208.1

Smagorinsky, J. 1963. General circulation experiments with the primitive equations: I. the basic experiment. *Mon. Wea. Rev.* 91(3), 99–164. DOI: https://doi.org/10.1175/1520-0493(1963)091<0099:GCEWTP>2.3.CO;2

Sommeria, G and **Deardorff, J.** 1977. Subgrid-scale condensation in models of nonprecipitating clouds. *J. Atmos. Sci.* 34(2): 344–355. DOI: https://doi.org/10.1175/1520-0469(1977)034<0344:SSCIMO>2.0.CO;2

Staal, A, Tuinenburg, OA, Bosmans, JH, Holmgren, M, van Nes, EH, Scheffer, M, Zemp, DC and **Dekker, SC.** 2018. Forest- rainfall cascades buffer against drought across the amazon. *Nature Climate Change.* 8(6): 539–543. DOI: https://doi.org/10.1038/s41558-018-0177-y

Stéfanon, M, Drobinski, P, D'Andrea, F and **de Noblet-Ducoudré, N.** 2012. Effects of interactive vegetation phenology on the 2003 summer heat waves. *J. Geophys. Res.* 117(D24). DOI: https://doi.org/10.1029/2012JD018187

Stevens, B. 2007. On the growth of layers of nonprecipitating cumulus convection. *J. Atmos. Sci.* 64(8): 2916–2931. DOI: https://doi.org/10.1175/JAS3983.1

Stevens, B, Satoh, M, Auger, L, Biercamp, J, Bretherton, CS, Chen, X, Düben, P, Judt, F, Khairoutdinov, M, Klocke, D, et al. 2019. Dyamond: the dynamics of the atmospheric general circulation modeled on non-hydrostatic domains. *Prog. Earth Planet. Sci.* 6(1): 1–17. DOI: https://doi.org/10.1186/s40645-019-0304-z

Tompkins, AM and **Semie, AG.** 2017. Organization of tropical convection in low vertical wind shears: Role of updraft

entrainment. *J. Adv. Model. Earth Syst.* 9(2): 1046–1068. DOI: https://doi.org/10.1002/2016MS000802

van Heerwaarden, CC and **Teuling, AJ.** 2014. Disentangling the response of forest and grassland energy exchange to heatwaves under idealized land–atmosphere coupling. *Biogeosciences.* 11(21): 6159– 6171. DOI: https://doi.org/10.5194/bg-11-6159-2014

Vivoni, ER. 2012. Diagnosing seasonal vegetation impacts on evapotranspiration and its partitioning at the catchment scale during smex04–name. *J. Hydrometeorol.* 13(5): 1631–1638. DOI: https://doi.org/10.1175/JHM-D-11-0131.1

Wang, G and **Eltahir, EA.** 2000. Modeling the biosphere–atmosphere system: The impact of the subgrid variability in rainfall interception. *J. Clim.* 13(16), 2887–2899. DOI: https://doi.org/10.1175/1520-0442(2000)013<2887:MTBAST>2.0.CO;2

Wolf, S, Keenan, TF, Fisher, JB, Baldocchi, DD, Desai, AR, Richardson, AD, Scott, RL, Law, BE, Litvak, ME, Brunsell, NA, et al. 2016. Warm spring reduced carbon cycle impact of the 2012 us summer drought. *Proc. Natl. Acad. Sci.* 113(21): 5880–5885. DOI: https://doi.org/10.1073/pnas.1519620113

Zängl, G, Reinert, D, Rípodas, P and **Baldauf, M.** 2015. The icon (icosahedral non-hydrostatic) modelling framework of dwd and mpim: Description of the non-hydrostatic dynamical core. *Quarterly Journal of the Royal Meteorological Society.* 141(687): 563–579. DOI: https://doi.org/10.1002/qj.2378

Zeng, Z, Piao, S, Li, LZ, Zhou, L, Ciais, P, Wang, T, Li, Y, Lian, X, Wood, EF, Friedlingstein, P, et al. 2017. Climate mitigation from vegetation biophysical feedbacks during the past three decades. *Nat. Clim. Change.* 7(6): 432–436. DOI: https://doi.org/10.1038/nclimate3299

TO CITE THIS ARTICLE:
Lee, J, Hohenegger, C, Chlond, A and Schnur, R. 2022. The Climatic Role of Interactive Leaf Phenology in the Vegetation-Atmosphere System of Radiative-Convective Equilibrium Storm-Resolving Simulations. *Tellus B: Chemical and Physical Meteorology*, 74(2022), 164–175. DOI: https://doi.org/10.16993/tellusb.26

Submitted: 26 January 2022 **Accepted:** 02 May 2022 **Published:** 21 June 2022

COPYRIGHT:
© 2022 The Author(s). This is an open-access article distributed under the terms of the Creative Commons Attribution 4.0 International License (CC-BY 4.0), which permits unrestricted use, distribution, and reproduction in any medium, provided the original author and source are credited. See http://creativecommons.org/licenses/by/4.0/.

Tellus B: Chemical and Physical Meteorology is a peer-reviewed open access journal published by Stockholm University Press.